Eurographics Symposium on Rendering 2024
E Garces and E. Haines
(Guest Editors)

Volume 43 (2024), Number 4

Practical Appearance Model for Foundation Cosmetics

Dario Lanza[1], Juan Raúl Padrón-Griffe[1], Alina Pranovich[2], Adolfo Muñoz[1], Jeppe Revall Frisvad[3] and Adrián Jarabo

[1]Universidad de Zaragoza-I3A, Spain
[2] Linköping University, Linköping, Sweden
[3] Technical University of Denmark, Denmark

Figure 1: *We propose a practical appearance model for foundation cosmetics that can be stacked on top of human skin. Left: Rendering of a white female character skin without makeup. Middle: We apply a* foundation *layer with a matte finish, which reduces the specular highlights, especially visible in the eye region and next to the nose, and slightly changes the skin color. Right: We apply an additional* shinier *layer adding a reddish tint to the cheek.*

Abstract

Cosmetic products have found their place in various aspects of human life, yet their digital appearance reproduction has received little attention. We present an appearance model for cosmetics, in particular for foundation layers, that reproduces a range of existing appearances of foundation cosmetics: from a glossy to a matte to an almost velvety look. Our model is a multilayered BSDF that reproduces the stacking of multiple layers of cosmetics. Inspired by the microscopic particulates used in cosmetics, we model each individual layer as a stochastic participating medium with two types of scatterers that mimic the most prominent visual features of cosmetics: spherical diffusers, resulting in a uniform distribution of radiance; and platelets, responsible for the glossy look of certain cosmetics. We implement our model on top of the position-free Monte Carlo framework, that allows us to include multiple scattering. We validate our model against measured reflectance data, and demonstrate the versatility and expressiveness of our model by thoroughly exploring the range of appearances that it can produce.

CCS Concepts

• ***Computing methodologies*** → ***Reflectance modeling;***

1. Introduction

Since ancient times, decorative cosmetics have been used in virtually all existing cultures around the globe. From the prehistoric mineral-based pigments [Wat09] to modern sophisticated chemical makeup, cosmetics have been used for enhancing appearance and hiding imperfections, for ritual painting, theatrical purposes, or most recently, visual effects. However, despite their ubiquity, cosmetics have not been explored much in graphics, most likely because they are generally baked into the look-development process for virtual humans. Rendering of cosmetics has received lit-

tle attention, limited to image-space [XDZ13, NL17, YGZ*23] or texture-space manipulation [SRH*11, YTK23], or simplistic physical models [HHLC13, LZL15, LZWL19]. Existing models either directly manipulate an image or describe how cosmetics modify the parameters of conventional analytic shading models. Our approach models the light-scattering particles in the cosmetic layer and computes the effect of such a layer using position-free Monte Carlo simulation.

Several types of cosmetics exist with different areas of application and intended goals. In the case of facial makeup, one or more relatively thin layers of cosmetics are applied on top of the skin, resulting in a multilayered structure. Facial makeup cosmetics, including *foundation*, *concealers*, *rougers* (*blusher*), *bronzers* and *highlighters*, consist of a combination of microscopic colored diffusers and platelets, either suspended in a water-based host medium, or presented as powder that sticks to the outermost sebum layer of the skin. At a macroscopic level, the diffusers and platelets interact with light as a scattering medium.

In this work, we focus on the base layer or *foundation*. A foundation aims to provide a uniform skin hue over the whole face upon which other makeup layers can be stacked. A key visual attribute of a foundation layer is its *finish*: Different foundation products exhibit distinct visual characteristics ranging from a *matte* finish that results in a non-shiny, velvety appearance; to a *dewy* finish that aims for a more natural appearance making the skin brighter and shinier to evoke an impression of a healthy skin.

Based on the observed types of appearance existing in foundation cosmetics, we propose an intuitive empirical appearance model for foundation makeup, where we model each cosmetic layer as a finite volumetric scattering layer, and where the bulk scattering properties are derived from a mixture of spherical-like and platelet-like scatterers. This enables us to stack an arbitrary number of makeup layers, resulting in a single bidirectional scattering distribution function (BSDF). We implement our model using the position-free Monte Carlo formalism [GHZ18], allowing for multiple scattering and arbitrary distributions.

Our model is able to reproduce a wide variety of appearances, from dewy to matte. We compare our model against measurements of real-world cosmetics, and show that our model closely fits such measurements, while reproducing the main visual features of cosmetics when applied on top of digital human skin. In addition, we show that our model can be used to model other types of cosmetics (e.g., blusher) and enables the stacking of multiple makeup layers as exemplified in Figure 1.

2. Related Work

Volumetric materials. Simulation of light scattering in a volume generally involves solving the radiative transfer equation [Cha60] or its variants for anisotropic [JAM*10] or correlated media [BRM*18, JAG18]. Based on this theoretical framework, numerous appearance models have been proposed for materials such as skin [Sta01, DWd*08, IGAJG15, AXX*23], paper [PdMJ14], cloth [ZJMB11, ZJA*23], leaves [BR01], special pigments [GMG*20], ice [FCJ07], wood [MWAM05, LDHM16], or granular media [MPH*15, MPG*16]. Our work follows this line of work and models foundation makeup as a combination of isotropic and anisotropic scatterers inside a scattering medium.

Multilayered materials. Early work on rendering of multilayered materials simulated the reflection and transmission by the multilayered structure of skin and leaves using subsurface scattering [HK93, DJ05], being limited to diffuse reflectance. Later work proposed using the adding-doubling method on spatio-angular scattering representations of thin slabs for stacks of isotropic [JdJM14] and anisotropic layers [ZJ18]. These methods require expensive precomputation and large storage requirements. On the other hand, approximate models have been successful in practice, due to their efficiency and simplicity [WW07, Bel18, WB20]; these methods follow the microfacets formalism, which makes them very suitable for integration in modern offline and real-time renderers, at the cost of reduced fidelity of the underlying light transport. A more accurate precomputation-free solution was proposed by Guo et al. [GHZ18] based on Monte Carlo random-walks inside the layered material; they leveraged a position-free formulation of light transport for providing bidirectional estimators of the BSDF, leveraging variance reduction via multiple importance sampling. This work was later extended to support more advanced sampling estimates [GGN20, XWHM20]. Previous work [WJHY22] proposed a different formulation for multilayered materials, by proposing index-matched layers. This significantly simplified the layer stacking, allowing for closed-form solutions for the single-scattering BRDF, and allowing simple learning-based multiple scattering approximations. This learning-based modeling of layered materials was further explored recently for all components of the BRDF [GLH*23]. In this work, we leverage multilayer material formulations for the modeling of our makeup BSDF. Specifically, we implement our model on top of position-free Monte Carlo [GHZ18], following the index-matched simplifications that previous work proposed [WJHY22] in the context of layered materials.

Visual reproduction of cosmetics. A considerable body of work on visual reproduction of cosmetics has focused on image-space makeup transfer [XDZ13, LOQ*16, CLYF18, LQD*18, SLL*20, JLG*20, DHC*21, WCA*22, YHXG22, LJG*22, YGZ*23]. Such works do not aim at characterizing the underlying properties of cosmetics but rather transfers an example of makeup from an input photograph to a target image, as in style-transfer methods. The facial appearance of a 3D model is usually described by textures. One way to encode makeup is to model how texture layers like diffuse, specular, and scattering albedo change when the cosmetic is applied [SRH*11, YTK23]. While these methods are useful for setting parameters in an analytic spatially-varying BRDF, like the conventional microfacet model [TS67], they do not enable us to compute the appearance of an applied cosmetic based on the constituents of the makeup material. With reflectance measurements from a gonioreflectometer one can fit a microfacet model to the data and use this to analyze the appearances of different cosmetics. This has been done for liquid foundation cosmetics [TM09, MTH09], and the researchers found that a data-driven model based on principal component analysis (PCA) provided a better representation of the data than the Torrance-Sparrow model. However, a data-driven BSDF does not lend itself to editing and representation of related

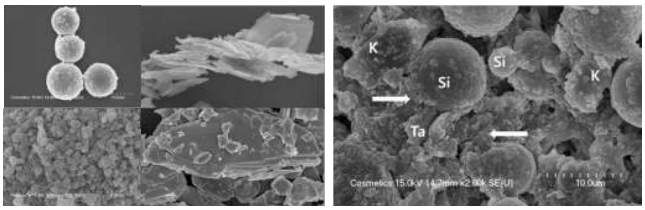

Natural State Product Powder Mixed

Figure 2: *Scanning electron microscope (SEM) image of different minerals in their natural state (left, in clockwise order): Silica, Talc, Kaolin and Titanium Dioxide. Note how Talc and Kaolin have a polygonal and plate-like geometry, while Silica and Titanium Dioxide have a more round or cubic shape. SEM image of the product powder mixed with the Sebum stratum (right). Courtesy of Jeon and Chang [JC12].*

materials. Closer to our work, Huang et al. [HHLC13] and Li et al. [LZL15, LZWL19] reproduced the appearance of a liquid foundation by modeling a cosmetic layer using Kubelka-Munk theory for the diffuse reflectance and transmittance of the layer and a microfacet model for its specular reflectance. However, as found in the PCA study, the conventional analytic microfacet BRDF model cannot accurately capture the directional distribution of the scattered light and the Kubelka-Munk theory is diffuse, .ie, there is no directional dependency. In contrast, we model the appearance of foundation makeup by computing the directional distribution of the light due to scattering by the different types of particles inside the layer.

3. Foundation Cosmetics

Foundation cosmetics, as well as other types of cosmetics (e.g., eyeshadows, lipsticks or primer), are generally made from a combination of colorants, minerals, vitamins and other chemicals included for skin health reasons [WSZT21]. A fundamental distinction between foundations is the base used for dispersing these constituents. *Liquid-based foundations* typically disperse these particles within a host medium such as water or silicone. As the majority of the particles are not soluble in the host medium (talc is not water-soluble, for example) the final system is colloidal, meaning that tiny particles are dispersed within the host medium. In contrast, *powder-based foundations* use the sebum stratum to bind these materials together, forming a layer in which cosmetic particles are mixed with the sebum [JC12]. Common colorants include minerals such as talc, kaolin, silica, or titanium dioxide, which are present as small powder-like particles with different shapes [JC12]. While minerals like kaolin and talc have flake-like polygonal geometry, titanium dioxide or silica tend to have spherical or cuboidal shapes (Figure 2). This difference in shape results in radically different scattering behaviour, leading to a different *finish* of the makeup. The color and finish are thus the two most important visual attributes for a correct reproduction of the appearance of a foundation layer.

Coloration Since foundation layers are used to create an even layer, the color and hue of the foundation have to roughly match the underlying skin hue, making colorants a key aspect of a foundation layer. Colorants can be categorized into two types: dyers, derived synthetically, and pigments, which have a biological origin. As colorants can have an impact on human health, efforts have been intensified to develop new technologies to ensure a stringent control of colorant concentration in cosmetic products [GCL*15, GLGJ17]. The main source of coloration is scattering and absorption, since regulations [BA09] do not allow coloration through photoluminescence or other chemical reactions. In addition, diffractive particles are allowed to be used as colorants in effect pigments [MPR05], though these are not common due to the need for running extra safety studies. We focus on the most common scattering-based colorants.

Finish Different foundations exhibit distinct visual characteristics ranging from a *matte* finish, resulting in a non-shiny, velvety appearance, to a *dewy* finish, aiming to achieve a more natural appearance that makes the skin brighter and shinier to evoke an impression of a healthy skin. The finish of a foundation layer is mainly caused by the concentration and shape of the different particles that constitute the bulk properties of the material, which directly affects the scattering behaviour. While flake-like particles scatter light more coherently, spherical particles scatter light in a more isotropic fashion, leading to a more matte appearance.

Summary The appearance of foundation cosmetics is the result of multiple scattering by a thin scattering medium, modeled by the combination of two types of scattering behaviour: On one hand, we can assume that diffusers are responsible for the diffusive look and incoherent backscattering in matte appearances, while more directional scatterers (such as platelets) model the more coherent scattering reflection responsible for the highlights prominent in dewy foundations. These are somewhat aligned with different types of particles used to produce foundation cosmetics. Based on these different types of observed type of scattering, in the following we present our model, defined using radiative transfer theory as a mixture of different scatterers in a scattering medium.

4. A BSDF for Foundation Cosmetics

As described in section 3, foundation cosmetics are applied as a layer on top of the skin, and its appearance is the result of the volumetric scattering in the layer. We model the layer statistically, as the combination of two uncorrelated scatterers uniformly distributed in the medium: spherical diffusers and anisotropic reflective platelets. Figure 3 shows a diagram of our model for a single foundation layer over the skin.

We assume elastic scattering, i.e., both the energy and scatterers numbers are conserved, and negligible wave-optical coherence in the multiple scattering component. In addition, given the small thickness of foundation layers, we assume no horizontal scattering, and therefore that light exits at the same position as it enters. Thus, we represent the foundation layer using a BSDF, defined as the result of all light-matter interactions occurring in the cosmetic for a ray of incident light at direction ω_i and exiting the surface at direction ω_o. Following Guo et al. [GHZ18] we model $f(\omega_i, \omega_o)$ using

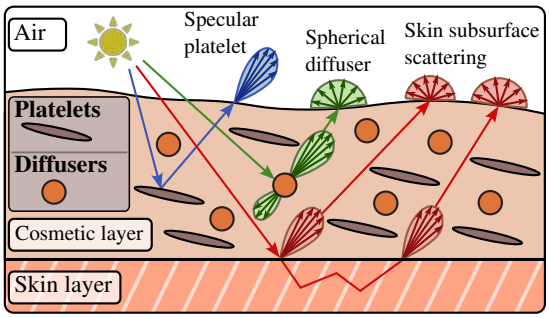

Figure 3: *We model a single foundation layer as a medium filled with two types of particles: platelets and spherical diffusers. Platelets generate specular lobes, using a more anisotropic phase function. In contrast, spherical diffusers generate rougher finishes, due to a more isotropic phase function. We account also for the subsurface scattering due to the underlying skin model.*

a position-free variant of the path integral as

$$f(\omega_i,\omega_o) = \int_{\Omega(\omega_i,\omega_o)} \Phi(\mathbf{x}) d\mu(\mathbf{x}), \tag{1}$$

with $\Omega(\omega_i,\omega_o)$ the space of light paths entering and exiting the differential surface at directions ω_i and ω_i respectively, $\Phi(\mathbf{x})$ the contribution of the path $\mathbf{x} \in \Omega(\omega_i,\omega_o)$ as the sequence of scattering and absorption events inside the foundation volumetric layer, and $\mu(\mathbf{x})$ the measure of path $\mathbf{x}$. By construction, the BSDF modeled by Equation (1) is energy conserving and reciprocal only if the scattering events conserve energy and are reciprocal. Table 1 lists all the parameters used in our model (BSDF), including both bulk and user parameters.

4.1. Optical properties of the foundation layer

We model the foundation layer as a statistical volumetric scattering plane-parallel layer with thickness t. To account for specular-like scattering, we describe light transport using the anisotropic radiative transfer framework [JAM*10], and describe radiance L in the direction of observation ω_o following

$$(\omega_o \cdot \nabla) L(\omega_o) + \sigma_t(\omega_o) L(\omega_o) = \sigma_s(\omega_o) \int_\Omega f_p(\omega_o \to \omega) L_i(\omega)\, d\omega, \tag{2}$$

with $\sigma_t(\omega_o)$ and $\sigma_s(\omega_o)$ the direction-dependent extinction and scattering coefficients, Ω the unit sphere of directions, $f_p(\omega_o \to \omega)$ the phase function, and $L_i(\omega)$ the incoming radiance in direction ω. Note that we omit the spatial and spectral dependencies for clarity, and assume that the source term is outside the scattering layer.

We assume a match of the indices of refraction of the particle host medium and the outside medium (as in powder-based foundations). The resulting absence of scattering and refraction at the interface allows for a simpler evaluation at render time and simplifies the parameterization of our model. Even liquid foundations tend to form a semi-dry film once applied. Most of the appearance is thus the result of the interaction with only the minerals and colorants. In Section 5 we validate this choice.

Parameter	Definition
η	Complex refractive index (=1)
t	Layer thickness
c_d	Diffuser particles concentration
Λ_d	Single scattering albedo for spherical diffusers
g_1, g_2	Anisotropy of diffuser's lobes
w_g	Weighting factor of diffuser's lobes
Λ_p	Single scattering albedo for platelets
α_p	Platelets roughness value
θ_p	Platelets rotation along the tangent direction

Table 1: *Parameters of our model for a single layer.*

Modeling the optical parameters The anisotropic RTE (2) is characterized by the extinction and scattering coefficients, $\Sigma_t(\omega_o)$ and $\Sigma_s(\omega_o)$, and the phase function $f_p(\omega \to \omega_o)$. We assume that the host medium has negligible effect on these optical properties, and thus only spherical diffusers and platelets are responsible for the appearance. This is reasonable since the thickness of foundation layers is usually small, and the layer is in a semi-dry state.

Building on top of the spatial uncorrelation assumption, we model the extinction coefficient as the combined probability of extinction for both diffusers $\sigma_\mathrm{d}(\omega_o)$ and platelets $\sigma_\mathrm{p}(\omega_o)$, following

$$\sigma_t(\omega) = \sigma_\mathrm{d}(\omega) + \sigma_\mathrm{p}(\omega) = N_\mathrm{d} C_\mathrm{d} + N_\mathrm{p} C_\mathrm{p}(\omega), \tag{3}$$

with N_d and N_p the number density of spherical diffusers and platelets in m^{-3}, respectively, and C_d and $C_\mathrm{p}(\omega)$ their extinction cross sections in m^2. Note that the extinction cross-section of the spherical diffusers has no dependency on the direction. To find practical user parameters, we model extinction as a function of a base extinction

$$\sigma_\mathrm{base} = \sigma_\mathrm{d} + N_p \max_\omega C_\mathrm{p}(\omega) \tag{4}$$

representing the non-directional part of the extinction coefficient for all the scattering particles in the material. To include the directional dependency, we use

$$\sigma_t(\omega) = \sigma_\mathrm{base} \left(c_\mathrm{d} + (1 - c_\mathrm{d}) \hat{C}_\mathrm{p}(\omega) \right), \tag{5}$$

with $\hat{C}_\mathrm{p}$ the normalized version of the extinction cross-section of the platelets and c_d the relative concentration of spherical diffusers out of the total concentration of particles:

$$\hat{C}_\mathrm{p}(\omega) = \frac{C_\mathrm{p}(\omega)}{\max_\omega C_\mathrm{p}(\omega)} \quad \text{and} \quad c_\mathrm{d} = \frac{\sigma_\mathrm{d}}{\sigma_\mathrm{base}}. \tag{6}$$

Since we do not include absorption in our model for computing the extinction cross-section and assume that all chromatic effects are due to absorption, our $C_p(\omega)$ has no spectral dependency. To introduce practical parameters for specifying the part not being absorbed, we use non-directional spectral single-scattering albedos for the spherical diffusers Λ_d and the platelets Λ_p. The single-scattering albedo is defined by $\Lambda(\omega) = \sigma_s(\omega)/\sigma_t(\omega)$, so we use the factors for diffuse and directional extinction in Equation 5 to model this:

$$\Lambda(\omega) = \frac{\Lambda_\mathrm{d} c_\mathrm{d} + \Lambda_\mathrm{p} (1 - c_\mathrm{d}) \hat{C}_\mathrm{p}(\omega)}{c_\mathrm{d} + (1 - c_\mathrm{d}) \hat{C}_\mathrm{p}(\omega)}. \tag{7}$$

Finally, we build our phase function as a linear blend of the phase functions of diffusers and platelets f_d and f_p, weighted by the total scattered light by each of the particles following

$$f(\omega \to \omega_o) = \frac{\Lambda_\mathrm{d}\, c_\mathrm{d}\, f_\mathrm{d}(\omega \to \omega_o) + \Lambda_\mathrm{p}\,(1-c_\mathrm{d})\,\hat{C}_\mathrm{p}(\omega)\, f_\mathrm{p}(\omega \to \omega_o)}{\Lambda_\mathrm{d}\, c_\mathrm{d} + \Lambda_\mathrm{p}\,(1-c_\mathrm{d})\,\hat{C}_\mathrm{p}(\omega)}. \quad (8)$$

This phase function is normalized if both f_d and f_p are normalized. The phase function is not reciprocal, but reciprocity is achieved due to $f(\omega \to \omega_o)\sigma_s(\omega) = f(\omega_o \to \omega)\sigma_s(\omega_o)$. Thus, our BSDF (1) is energy-conserving and reciprocal. In the following, we detail the scattering behaviour of both diffusers and platelets, and the implementation of our model.

4.2. Scattering by Diffusers

Following the measurements by Wang et al. [WXN*19], who analyze colloidal systems made of nanoscopic titanium dioxide particles, we use a mixture of phase functions to model the scattering of diffusers. This is common practice in computer graphics and related areas [GXZ*13, DHV*23, d'E16]. In particular, we model the scattering from diffusers using a mixture of two Henyey-Greenstein lobes $f_\mathrm{HG}(\omega \to \omega_o | g)$ each parameterized by the mean cosine of the scattering angle g [HG41]. This is similar to previous work modeling the scattering of sunscreen lotions [NNN*22]. The resulting phase function is

$$f_\mathrm{d}(\omega \to \omega_o) = w_g f_\mathrm{HG}(\omega \to \omega_o | g_1) + (1-w_g) f_\mathrm{HG}(\omega \to \omega_o | g_2), \quad (9)$$

with $w_g \in [0,1]$ the blending parameter between the two lobes.

4.3. Scattering by Platelets

To reproduce the glossy appearance required by a dewy finish, we use platelet particles, i.e., flat particles suspended in the medium that generate a glossy reflection. Platelets are purely reflective micro-flakes [JAM*10] suspended in the medium, following the SGGX distribution of normals $D_\mathrm{SGGX}(\omega_m)$ [HHdD16], with ω_m the microflake normal.

We assume a disk-like distribution of platelets, and parametrize $D_\mathrm{SGGX}(\omega_m)$ by a roughness α_p parameter along the distribution's mean direction, and a rotation angle θ_p that rotates the mean direction of the distribution with respect to the tangent direction of the surface, so that the distribution does not need to be aligned with the surface normal.

The distribution of normals $D_\mathrm{SGGX}(\omega_m)$ directly enables us to compute the projected area of the platelets, which we, as in previous work [JAM*10, HDCD15], assume equal to $\hat{C}_\mathrm{p}(\omega)$. As phase function, we opt for a specular SGGX phase function without Fresnel effects, so that the phase function for platelets is defined by

$$f_\mathrm{p}(\omega \to \omega_o) = \frac{D_\mathrm{SGGX}(\omega_h)}{4\hat{C}_\mathrm{p}(\omega)}, \quad (10)$$

with $\omega_h = (\omega + \omega_o)/\|\omega + \omega_o\|$ the half vector.

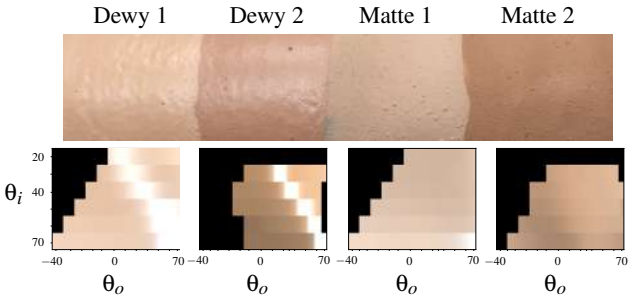

Figure 4: *Measured samples (top row), wrapped around a cylinder for demonstration purposes. Reflectance profile measured with our setup (bottom row), with angles of observation θ_o on the horizontal axis and angles of incidence θ_i on the vertical axis. Negative angles of observation represent retro-reflectance configurations. Black pixel areas indicate that no information was available.*

4.4. Implementation & Properties

We implemented our model in PBRT v4 [PJH23] on top of the position-free Monte Carlo framework from Guo et al. [GHZ18]. This allows us to compute multiple scattering as an average of random walks inside the layer with next-event estimation for variance reduction, and to easily stack multiple layers of cosmetics. The source code, scenes and reflectance measurements are available on the project page.

We compute Equation (1) using a Monte Carlo estimate, by randomly sampling paths starting at direction ω_i. We build the random walk by using exponential mean free path sampling with $\mathrm{pdf}(s) = \sigma_t(\omega)\exp(-\sigma_t(\omega)\,s)$. A collision is found as long as the sampled distance s remains inside the layer. Otherwise, we move to the contiguous layer (the skin or outside). At each interaction inside the medium, we select a lobe (platelet or one of the two Henyey-Greenstein lobes) using Shirley's remapping [SLH*19] (with probabilities driven by c_d and w_g). Then, platelets are sampled using SGGX visible normals sampling [HDCD15], while Henyey-Greenstein phase functions are sampled using the usual CDF-inversion-based routine. Absorption is handled by multiplying the throughput by the single-scattering albedo (Equation 7) at each bounce. To reduce variance, we only use Russian Roulette as a path termination criterion after 128 bounces. The sampling routines and PDF functions are evaluated following PFMC [GHZ18], using a forward path sampling inside the medium, with PDF the probability density of generating the path.

5. Analysis and Evaluation

In this section, we validate our model against measurements of cosmetics reflectance. We capture the reflectance from four liquid-based foundations from *Clarins*, with varying colors and finishes, from dewy to matte. In particular, we select *Skin Illusions 105 Nude* (Dewy 1), *Skin Illusions 112 Nude* (Dewy 2), *Skin Illusions Velvet 103 Nude* (Matte 1) and *Skin Illusions Velvet 108* (Matte 2). We show samples for each of them in Figure 4, top row.

5.1. Sample Preparation

We captured the reflectances using a home-built setup, consisting of a gonioreflectometer, a light source (Xenon lamp emitting in about 6200K temperature), and an Ocean Optics spectrometer with fibre input and an attached collecting lens, as shown in Figure 5. We directed a collimated beam with a diameter of 4 mm onto the sample. The direction of incidence was explored by rotating the sample holder, and the direction of observation by independently rotating the receiver's arm. Reflectance values were estimated by dividing the received spectral values by the signal reflected from a white reference, a 99% spectralon by Labsphere. Calibration with spectralon additionally compensates for the geometrical foreshortening [War92]. We collected our measurements on a flat black slab made of matte polymer, which we found easier to calibrate than synthetic skin, and that simplified the layer beneath the cosmetic, which was useful for optimization. We could not directly measure the thickness of the samples, however, we performed several measurements on a silicon plate (mirror) to validate that we were in the multiple scattering regime. We added thin layers of the cosmetic product until we found no difference in measurements with respect to the number of layers.

In preparation for our samples, we applied a thick layer of cosmetic product on a black substrate. This is different from previous work [MTH09], where measured cosmetics were applied on top of synthetic skin that might interfere with the cosmetic's reflectance data. We measure our samples in a semi-dry state, leaving them resting for an hour to allow the formation of a homogeneous layer. This resembles better the condition of a product when it is applied since usually a small quantity of product is spread over a comparatively large surface. Air exposition is likely to evaporate the product into a semi-dry state. This mechanism might also impact the hue of the product [YLHS20].

5.2. Captured Data

Figure 4 shows the captured data for our four liquid foundations. We plot measured data as sRGB- colored patches to better visualize the color and highlight shape changes. As we sparsely gather measurements we linearly interpolate between measurements and leave black pixels to represent lack of data. We measure both forward and backscattering for all products, although our setup does not allow us to measure for all light-view configurations, in some cases due to low a signal-to-noise ratio.

We only capture the inclination angle and not azimuthal data as our setup did not allow it. However, we believe that this is not a major issue since cosmetics are often applied on the skin without following any precise stroke direction, but rather in a circular manner, precisely to hide any anisotropy. Therefore, it is reasonable to assume that a small amount of reflectance changes occurs in the azimuthal plane and that most of the changes in appearance happen along the inclination angle.

As seen in Figure 4, the selected samples exhibit different reflectance behaviors: Dewy 1 and Dewy 2 displays a dewy finish, characterized by sharp highlights. Matte 1 can be considered an intermediate foundation, similar to a velvet finish, showing highlights

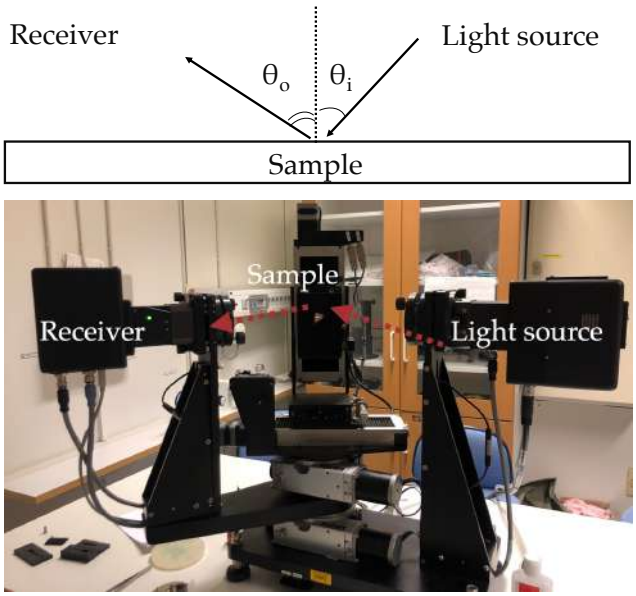

Figure 5: *Experimental setup for measuring reflectance. We modify a commercial gonioreflectometer to collect spectral reflectance in non-specular directions.*

for only grazing angles. In contrast, Matte 2, is clearly matte (absence of highlights). In all cases, we found some backscattering, in agreement with previous work [MTH09].

5.3. Comparison between model and captured data

To analyze how accurately our model can represent the actual appearance of cosmetics, we fit our model to the measured data for each of the four samples, by solving

$$\underset{\boldsymbol{\pi}_i}{\operatorname{argmin}} \sum_{(\theta_i,\theta_o)\in M} d\left(I(\theta_i,\theta_o), f_s(\theta_i,\theta_o,\boldsymbol{\pi}_i)\right), \tag{11}$$

where $\boldsymbol{\pi}_i$ is the appearance model parameters (see Section 4), $I(\theta_i,\theta_o)$ is the measured data in linear RGB space at incoming angle θ_i and outgoing angle θ_o, $f_s(\theta_i,\theta_o,\boldsymbol{\pi}_i)$ is our BSDF, and $d(\cdot,\cdot)$ is the L_2 distance metric. Our model is evaluated using Monte Carlo integration as described in Section 4. We use a derivative-free optimizer (modified Powell algorithms from the SciPy library); since this approach is sensitive to initialization we first perform a manual selection of the parameters and then use the optimizer to refine the solution. We use the L2 distance function in linear RGB space, although we show the results in sRGB space. We prepared the digital replica by setting the underlying layer as a black Lambertian surface and set the foundation layer thickness to 16 optical depths to enforce the multiple scattering conditions in which samples were taken. Computation-wise, we limit the number of bounces to 512, we then sample each direction 128 times. We evaluated this setup with preliminary experiments and found that it offered a good trade-off between time of execution and energy loss. We run the optimization described, allowing the model to optimize also for the IoR and surface roughness parameters (using the Trowbridge-Reitz distribution). At the end of the optimization cycle, we found values

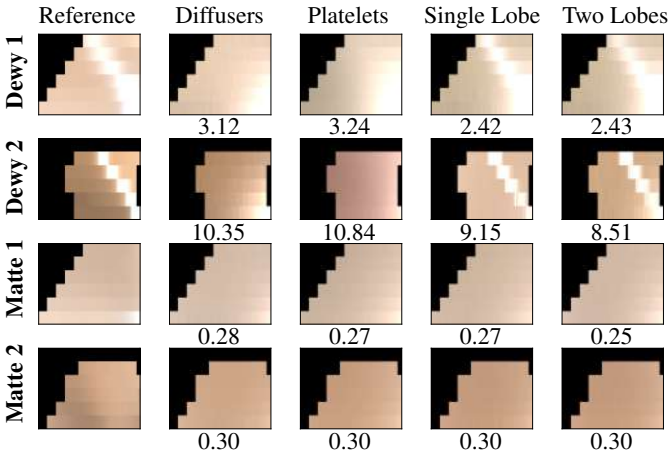

Figure 6: *Ablation study results: reference data from measured samples (first column), media composed only of diffuser particles (second column), media made of only platelet particles (third column), media with both types of particles (diffusers and platelets) with a single lobe phase function and our full model (last column). For each configuration, we report the error under the L2 distance. Notice how the models using only one type of particle cannot approximate well both types of appearances (matte and dewy) and the full model overall exhibits the lowest error across all the products.*

close to 1.0 for the index of refraction, thus supporting the validity of our interface-free simplification of the medium, which allows us to further reduce the number of parameters and reduces the computational cost by removing an interface from the computations.

Figure 6 shows the results of the optimization process for the four samples (last row), among the error measured under the L2 loss function. Our model captures the general behavior of the measured data in terms of reflected energy, color and highlight shapes. Some small differences are present in the intensity gradients of the diffuse part of the darker samples at grazing angles (Matte 2 and Dewy 2). We discuss these differences in Section 7.

Ablation study. We ran an ablation study of our model to examine the effect of its various components. Using the approach discussed above, we optimized three incremental versions of our proposed model: One composed of spherical diffusers only (Diffusers Only), one that is composed of platelets only (Platelets Only), and one that uses both particles but with a single lobe for the spherical diffuser particles (Full, Single Lobe). We initialize the optimization of each variation using the fitted parameters of our full model (Full, Two Lobes). Figure 6 shows the results of this ablation study: It demonstrates that a model with only one particle type, either diffusers or platelets, is unable to properly reproduce the highlights of glossy appearances (Dewy 1 and Dewy 2). The reason is that one type cannot simultaneously generate highlights at grazing angles and in near-specular directions. In contrast, the combination of both particles with single-lobe diffusers generates results that are comparable with our full model, except for minor hue differences in Dewy 2. This suggests that a model with single-lobe diffusers could be sufficient to represent some real-world cosmetics, at the cost of losing expressivity, as we show in the next section.

6. Results

In this section, we visually analyze our model in realistic use cases. We implemented our model as a layered material in PBRT v4 [PJH23]. For the base skin, we use the random-walk-based default PBRT skin model. We first demonstrate our model using the realistic materials captured in the previous section; then we analyze the appearance space defined by the parameters of our model.

We report rendering times and sample counts, in addition to the user parameters obtained through optimization of the measured foundations, in Appendix A.

Captured data Figure 7 shows our model with the parameters obtained from captured data, applied on top of the PBRT skin model. As expected, while the two dewy foundations enhance the highlights, matte foundations remove the highlights. Note how both dewy and matte foundations also slightly reduce the effect of skin subsurface scattering.

In Figure 8, we qualitatively evaluate our model against pictures of cosmetics applied on real skin. Our model reproduces the trends shown in the pictures: an increase in reflection when Dewy 1 is applied to the skin, and a more matte appearance, especially at grazing angles, for Matte 2.

Appearance exploration Figure 9 (a) explores the effect of the concentration of diffusers c_d and the thickness t (in mean-free-path units). In this experiment, we use a single phase function for the spherical diffusers. Increasing the thickness reduces the effect on the appearance of the underneath layer, while increasing the concentration of platelets (smaller c_d) increases the glossiness of the skin. In contrast, when increasing c_d the appearance shifts to matte, as expected. The reason for brighter highlights with increasing thickness in dewy foundations was observed by Yoshida et al. [YO21], where the authors explained that multiple applications of cosmetics lead to an increase in the reflected light. We have to clarify that this is not necessarily a general characteristic of all cosmetics, but rather a behavior that is shown by a certain subset of products.

In Figure 9 (b), we investigate the influence of c_d and α_p, the concentration of diffusers and the roughness of the platelets. We see that both parameters alter the perception of glossiness, although in different ways. While c_d affects the intensity of the highlights, α_p alters the shape of the highlights, going from sharper to broader highlights. Similar to before, these phenomena can be explained by observing that increasing c_d only decreases the chances of hitting a platelet, without altering the scattering behavior of the particle itself. On the other hand, α_p affects the scattering behavior of the particle, with rougher appearances obtained for bigger particles. We believe that these two parameters, c_d, and α_p can be helpful during editing, as they allow artists to edit two different dimensions of gloss perception, contrast, and sharpness of the highlight [PFG00].

We investigate the influence of using one or two-lobed phase functions in Figure 9(c) to see how t and c_d alter the appearance when diffusers are modeled with different phase functions. We observe that when diffusers are defined with a two-lobed phase function, the same parameters yield darker and more saturated colors. This can be explained by noting that when having two strongly

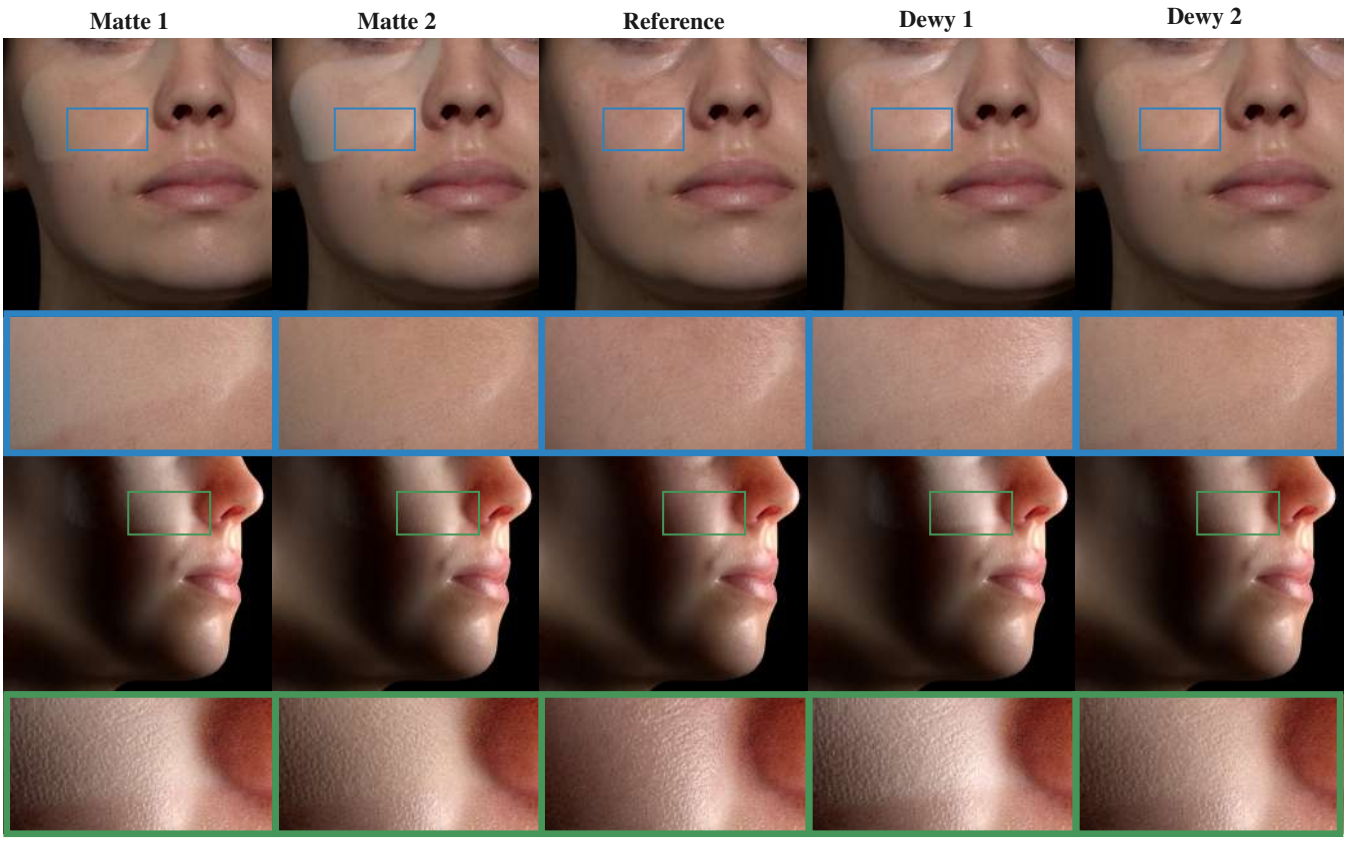

Figure 7: *Analysis of our model applied over realistic skin. In the first row, we show the effect that cosmetics have on highlights. As can be seen in the insets (blue boxes), the matte cosmetics tend to reduce the brightness of highlights, while the two dewy products enhance them. In the second row, we show how a layer of cosmetics affects the subsurface scattering of the underlying skin. In each column, we apply the optical parameters retrieved for each product.*

Figure 8: *We compare renderings obtained with our model (right) with photographs (left) of cosmetics applied over bare skin on the forehead. In both renderings and pictures, we apply the cosmetic on the left side of the forehead, leaving the right side with bare skin for reference. Our model captures the subtle increase in reflectance when Dewy 1 is applied (central area of the forehead). On the other hand, the model is also capable of generating a matte appearance for grazing angles when Matte 2 is applied.*

anisotropic lobes, light tends to be either forwarded or backscattered, thus resulting in a darker appearance, since less light gets scattered horizontally.

As expected, the influence of the skin layer is greater for small thickness values, while for higher values the appearance converges to a similar result, regardless of the appearance of the skin.

In Figure 10, we explore the capabilities of our model to reproduce the adequate hue for different skin types, for different product types. In each row, we apply four cosmetics strips, with only one of them matching the hue of the underlying skin type. This illustrates how a cosmetic product that does not match the hue of the underlying skin can be easily spotted. We run this experiment for both dewy and matte foundations, showing that our model is capable of generating an adequate hue for the different types of products. Matte cosmetics, as expected, provide a closer color match, while dewy foundations provide more desaturated colors in exchange for increased highlights

We also observe that the effect of glossiness is more prominent for darker skin tones, as observed in previous work on glossiness perception [PFG00]. This is a key aspect that has to be considered for different skin types.

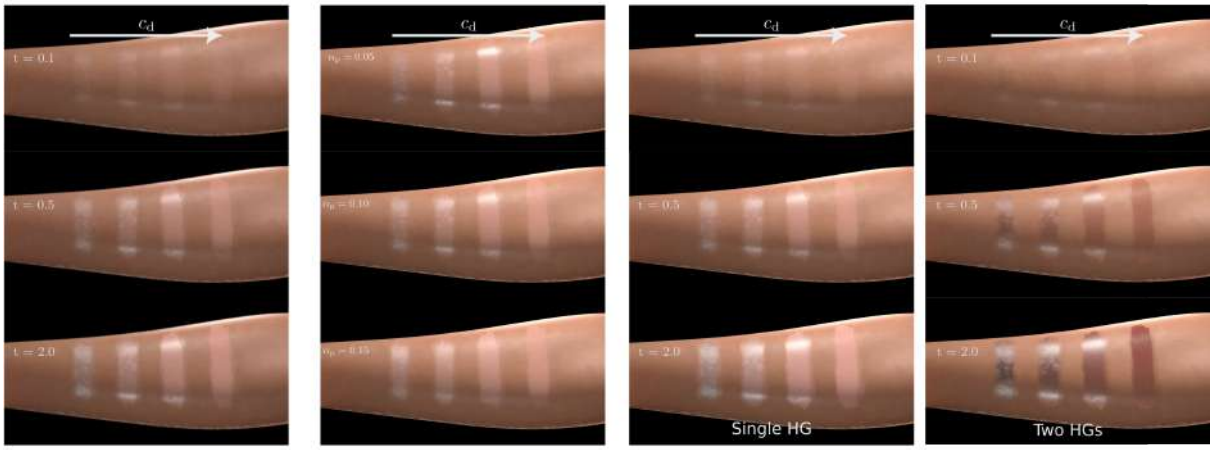

(a) Thickness vs Concentration (b) Roughness vs Concentration (c) single lobe vs two lobed

Figure 9: *Appearance exploration: we investigate the influence of the parameters of our model on the final appearance. In (a) we show the influence of thickness t and concentration of diffusers c_d. Thickness has a major impact on perceived reflectance. In (b) we explore the visual impact of α_p, the roughness of platelets, and c_d on the shape and brightness of highlights. α_p mainly affects the shape of the highlights, while c_d alters their intensity. In (c) we study the effect of using a single or a two-lobed phase function for diffusers. Two-lobed phase functions generate darker and more saturated appearances.*

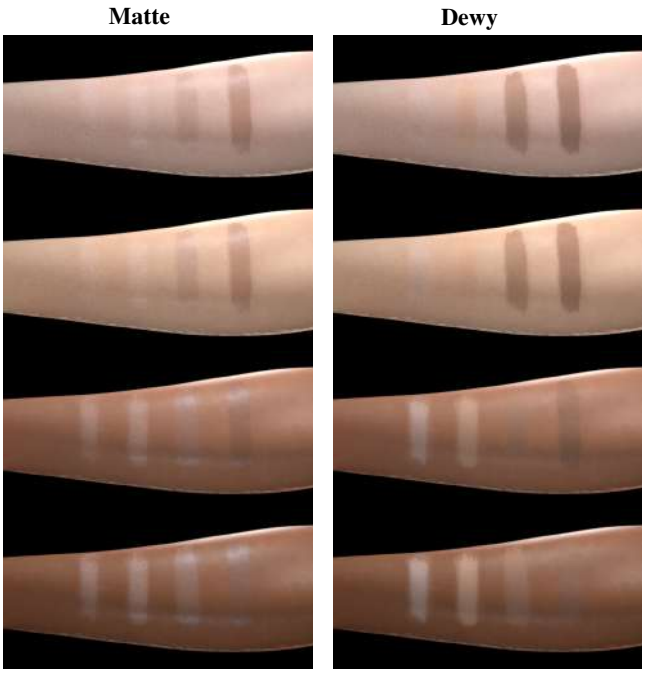

Figure 10: *Experiment matching the hue of different skin types. In each row, we simulate different cosmetic strips aimed to match the hue of different skin types. We apply the same cosmetics to all rows changing the underneath skin type. Note how incorrect hues can be easily spotted if not applied to the correct skin type. We repeat this experiment for the two categories of matte and dewy cosmetics. All results are obtained using $t = 0.5$.*

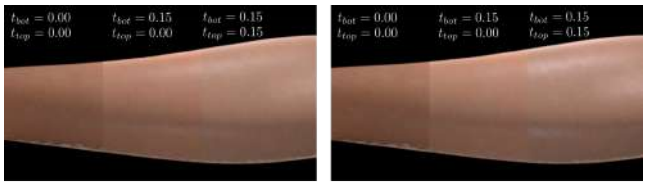

(a) bottom: dewy - top: matte (b) bottom: matte - top: dewy

Figure 11: *Effect of stacking two layers of foundation. (a) The bottom layer uses a dewy foundation, while the top layer is composed of a matte foundation. In (b) the bottom layer uses a matte foundation, while the top layer is a dewy foundation. Note how the topmost material dominates the final appearance.*

Finally in Figure 11, we explore the results of applying layers of foundations characterized by different final appearances. We run this experiment by taking dewy and matte foundation cosmetics and observing how they interact with each other depending on the order in which they are applied. We observe that the topmost layer dominates the final appearance. This is expected as the brightness of highlights is dominated by the first bounce, therefore the first few bounces are key in determining the final appearance.

7. Conclusions

We proposed a scattering model for characterizing cosmetic material using colored volumetric spherical diffusers and platelet particles. We demonstrated that this model is capable of reproducing the main characteristics of foundation layers by fitting the model to measured bidirectional reflectance data of sample products. We investigated the appearance space that our model spans, confirming that is possible to achieve believable results with our model. As op-

posed to previous work, we offer a model that can be easily edited and used to predict different appearances without necessarily being entangled with the skin type on which it was applied. We believe that our model offers a solid base but additional work is required to capture all the subtle nuances of cosmetic materials.

Strictly speaking, our model focuses on foundation makeup, and we have only validated it against this type of cosmetics. However, as shown in Figure 1, we can use our model to replicate the look of other types of makeup, which shows the versatility of our approach. Nevertheless, a more thorough analysis against measurements would be required for validating other ranges of cosmetics. Note also that the foundation samples are specific for light skin; however, as shown in Figure 10 our model is able to qualitatively capture the appearance of cosmetics targeting other skin types. Particularly interesting for future work is to investigate reflectance models for foundation layers that incorporate glittering effects. However, measuring this class of materials can prove to be a challenging task, as it is not clear how to measure the reflectance of a material that glitters if not by taking the aggregated behavior. An additional limitation is that our model builds upon pure ray optics, and thus it ignores diffraction effects occurring due to the powder-like nature of the scatterers. That might explain why our model is not able to fully reproduce the reflectance behavior exhibited by Dewy 2, which we hypothesize is caused by the interference caused at grazing angles observed in previous work for different materials [LKYU12,EBM18]. Adding a diffraction reflection lobe [HP17] could help our model better fit the captured data and appearance behavior at grazing angles, and we think it is an interesting research direction for future work.

Studying the effect of heterogeneous and uncorrelated scatterers is an interesting avenue for future work as concurrent work shows that varying pigments radius and mass fraction can have a significant impact on the colored appearance of cosmetics [TLAV23]. Nevertheless, we found that using the classical RTE formulation for uncorrelated media fits well with measurements, while it also reduces the additional complexity of specifying non-exponential mean-free-paths.

In terms of implementation, our model is based on the PFMC framework, which requires several samples to converge to a noise-free solution. Implementing our model using faster position-free approaches [Bd22] or using the SpongeCake model [WJHY22] should be trivial, and would likely reduce significantly the overhead of our method. Finally, our model focuses on the local microscopic appearance of cosmetics, and thus does not account for the mesoscopic effects of cosmetics masking small crevices or pores which should change the normal or displacement mapping modeling of the skin mesogeometry.

References

[AXX*23] ALIAGA C., XIA M., XIE X., JARABO A., BRAUN G., HERY C.: A hyperspectral space of skin tones for inverse rendering of biophysical skin properties. *Computer Graphics Forum 42*, 4 (2023), e14887. doi:10.1111/cgf.14887. 2

[BA09] BUZEK J., ASK B.: Regulation (ec) no 1223/2009 of the european parliament and of the council of 30 november 2009 on cosmetic products. https://www.eumonitor.eu/9353000/1/j9vvik7m1c3gyxp/vibn2mp7slr0, 2009. 3

[Bd22] BITTERLI B., D'EON E.: A position-free path integral for homogeneous slabs and multiple scattering on Smith microfacets. *Computer Graphics Forum 41*, 4 (2022), 93–104. doi:10.1111/cgf.14589. 10

[Bel18] BELCOUR L.: Efficient rendering of layered materials using an atomic decomposition with statistical operators. *ACM Transactions on Graphics 37*, 4 (2018), 73:1–73:15. doi:10.1145/3197517.3201289. 2

[BR01] BARANOSKI G. V. G., ROKNE J. G.: Efficiently simulating scattering of light by leaves. *The Visual Computer 17*, 8 (2001), 491–505. doi:10.1007/s003710100126. 2

[BRM*18] BITTERLI B., RAVICHANDRAN S., MÜLLER T., WRENNINGE M., NOVÁK J., MARSCHNER S., JAROSZ W.: A radiative transfer framework for non-exponential media. *ACM Trans. Graph. 37*, 6 (2018), 225:1–225:17. doi:10.1145/3272127.3275103. 2

[Cha60] CHANDRASEKHAR S.: *Radiative Transfer*. Dover Publications, New York, 1960. doi:10.1002/qj.49707633016. 2

[CLYF18] CHANG H., LU J., YU F., FINKELSTEIN A.: PairedCycleGAN: asymmetric style transfer for applying and removing makeup. In *Computer Vision and Pattern Recognition (CVPR)* (2018), IEEE, pp. 40–48. doi:10.1109/CVPR.2018.00012. 2

[d'E16] D'EON E.: A hitchhiker's guide to multiple scattering, 2016. URL: https://eugenedeon.com/hitchhikers. 5

[DHC*21] DENG H., HAN C., CAI H., HAN G., HE S.: Spatially-invariant style-codes controlled makeup transfer. In *Computer Vision and Pattern Recognition (CVPR)* (2021), IEEE, pp. 6549–6557. doi:10.1109/CVPR46437.2021.00648. 2

[DHV*23] DROSKE M., HANIKA J., VORBA J., WEIDLICH A., SABBADIN M.: Path tracing in production: the path of water. In *ACM SIGGRAPH 2023 Courses* (7 2023), ACM. doi:10.1145/3587423.3595519. 5

[DJ05] DONNER C., JENSEN H. W.: Light diffusion in multi-layered translucent materials. *ACM Transactions on Graphics 24*, 3 (2005), 1032–1039. doi:10.1145/1073204.1073308. 2

[DWd*08] DONNER C., WEYRICH T., D'EON E., RAMAMOORTHI R., RUSINKIEWICZ S.: A layered, heterogeneous reflectance model for acquiring and rendering human skin. *ACM Transactions on Graphics 27*, 5 (2008), 140:1–140:12. doi:10.1145/1409060.1409093. 2

[EBM18] EWING B. E., BUTLER S. D., MARCINIAK M. A.: Improved grazing angle bidirectional reflectance distribution function model using Rayleigh–Rice polarization factor and adaptive microfacet distribution function. *Optical Engineering 57*, 10 (2018), 105102. doi:10.1117/1.OE.57.10.105102. 10

[FCJ07] FRISVAD J. R., CHRISTENSEN N. J., JENSEN H. W.: Computing the scattering properties of participating media using Lorenz-Mie theory. *ACM Transactions on Graphics 26*, 3 (July 2007), 60:1–60:10. doi:10.1145/1275808.1276452. 2

[GCL*15] GUERRA E., CELEIRO M., LAMAS J. P., LLOMPART M., GARCIA-JARES C.: Determination of dyes in cosmetic products by micro-matrix solid phase dispersion and liquid chromatography coupled to tandem mass spectrometry. *Journal of Chromatography A 1415* (10 2015), 27–37. doi:10.1016/j.chroma.2015.08.054. 3

[GGN20] GAMBOA L. E., GRUSON A., NOWROUZEZAHRAI D.: An efficient transport estimator for complex layered materials. *Computer Graphics Forum 39*, 2 (2020), 363–371. doi:10.1111/cgf.13936. 2

[GHZ18] GUO Y., HAŠAN M., ZHAO S.: Position-free Monte Carlo simulation for arbitrary layered BSDFs. *ACM Transactions on Graphics 37* (12 2018), 1–14. doi:10.1145/3272127.3275053. 2, 3, 5

[GLGJ17] GUERRA E., LLOMPART M., GARCIA-JARES C.: Miniaturized matrix solid-phase dispersion followed by liquid chromatography-tandem mass spectrometry for the quantification of synthetic dyes in cosmetics and foodstuffs used or consumed by children. *Journal of Chromatography A 1529* (12 2017), 29–38. doi:10.1016/j.chroma.2017.10.063. 3

[GLH*23] GUO J., LI Z., HE X., WANG B., LI W., GUO Y., YAN L.-Q.: MetaLayer: a meta-learned BSDF model for layered materials. *ACM Transactions on Graphics 42*, 6 (2023), 222:1–222:15. doi:10.1145/3618365. 2

[GMG*20] GUILLÉN I., MARCO J., GUTIERREZ D., JAKOB W., JARABO A.: A general framework for pearlescent materials. *ACM Transactions on Graphics 39*, 6 (2020), 253:1–253:15. doi:10.1145/3414685.3417782. 2

[GXZ*13] GKIOULEKAS I., XIAO B., ZHAO S., ADELSON E. H., ZICKLER T., BALA K.: Understanding the role of phase function in translucent appearance. *ACM Trans. Graph. 32*, 5 (2013). doi:10.1145/2516971.2516972. 5

[HDCD15] HEITZ E., DUPUY J., CRASSIN C., DACHSBACHER C.: The SGGX microflake distribution. *ACM Transactions on Graphics 34* (7 2015), 48:1–48:11. doi:10.1145/2766988. 5

[HG41] HENYEY L. G., GREENSTEIN J. L.: Diffuse radiation in the galaxy. *The Astrophysical Journal 93* (1941), 70–83. doi:10.1086/144246. 5

[HHdD16] HEITZ E., HANIKA J., D'EON E., DACHSBACHER C.: Multiple-scattering microfacet bsdfs with the smith model. *ACM Transactions on Graphics (TOG) 35* (2016), 1 – 14. doi:10.1145/2897824.2925943. 5

[HHLC13] HUANG C.-G., HUANG T.-S., LIN W.-C., CHUANG J.-H.: Physically based cosmetic rendering. *Computer Animation and Virtual Worlds 24*, 3-4 (2013), 275–283. doi:10.1002/cav.1523. 2, 3

[HK93] HANRAHAN P., KRUEGER W.: Reflection from layered surfaces due to subsurface scattering. In *SIGGRAPH '93* (1993), ACM, pp. 165–174. doi:10.1145/166117.166139. 2

[HP17] HOLZSCHUCH N., PACANOWSKI R.: A two-scale microfacet reflectance model combining reflection and diffraction. *ACM Trans. Graph. 36*, 4 (jul 2017). doi:10.1145/3072959.3073621. 10

[IGAJG15] IGLESIAS-GUITIAN J. A., ALIAGA C., JARABO A., GUTIERREZ D.: A biophysically-based model of the optical properties of skin aging. *Computer Graphics Forum 34*, 2 (2015), 45–55. doi:10.1111/cgf.12540. 2

[JAG18] JARABO A., ALIAGA C., GUTIERREZ D.: A radiative transfer framework for spatially-correlated materials. *ACM Trans. Graph. 37*, 4 (2018), 1–13. doi:10.1145/3197517.3201282. 2

[JAM*10] JAKOB W., ARBREE A., MOON J. T., BALA K., MARSCHNER S.: A radiative transfer framework for rendering materials with anisotropic structure. *ACM Transactions on Graphics 29*, 4 (2010), 53:1–53:13. doi:10.1145/1778765.1778790. 2, 4, 5

[JC12] JEON M.-O., CHANG B.-S.: Property of silica and fine structure of cosmetic white powders. *Applied Microscopy 42* (2012), 87–93. doi:10.9729/AM.2012.42.2.087. 3

[JdJM14] JAKOB W., D'EON E., JAKOB O., MARSCHNER S.: A comprehensive framework for rendering layered materials. *ACM Transactions on Graphics 33*, 4 (2014), 1–14. doi:10.1145/2601097.260113. 2

[JLG*20] JIANG W., LIU S., GAO C., CAO J., HE R., FENG J., YAN S.: PSGAN: pose and expression robust spatial-aware GAN for customizable makeup transfer. In *Computer Vision and Pattern Recognition (CVPR)* (2020), IEEE, pp. 5194–5202. doi:10.1109/CVPR42600.2020.00524. 2

[LDHM16] LIU A. J., DONG Z., HAŠAN M., MARSCHNER S.: Simulating the structure and texture of solid wood. *ACM Transactions on Graphics 35*, 6 (2016), 170:1–170:11. doi:10.1145/2980179.2980255. 2

[LJG*22] LIU S., JIANG W., GAO C., HE R., FENG J., LI B., YAN S.: PSGAN++: robust detail-preserving makeup transfer and removal. *IEEE Transactions on Pattern Analysis and Machine Intelligence 44*, 11 (2022), 8538–8551. doi:10.1109/TPAMI.2021.3083484. 2

[LKYU12] LÖW J., KRONANDER J., YNNERMAN A., UNGER J.: Brdf models for accurate and efficient rendering of glossy surfaces. *ACM Trans. Graph. 31*, 1 (feb 2012). doi:10.1145/2077341.2077350. 10

[LOQ*16] LIU S., OU X., QIAN R., WANG W., CAO X.: Makeup like a superstar: deep localized makeup transfer network. In *International Joint Conference on Artificial Intelligence (IJCAI)* (2016), AAAI Press, pp. 2568–2575. URL: https://www.ijcai.org/Proceedings/16/Papers/365.pdf. 2

[LQD*18] LI T., QIAN R., DONG C., LIU S., YAN Q., ZHU W., LIN L.: BeautyGAN: instance-level facial makeup transfer with deep generative adversarial network. In *Multimedia (MM '18)* (2018), ACM, pp. 645—-653. doi:10.1145/3240508.3240618. 2

[LZL15] LI C., ZHOU K., LIN S.: Simulating makeup through physics-based manipulation of intrinsic image layers. In *Computer Vision and Pattern Recognition (CVPR)* (2015), pp. 4621–4629. doi:10.1109/CVPR.2015.7299093. 2, 3

[LZWL19] LI C., ZHOU K., WU H.-T., LIN S.: Physically-based simulation of cosmetics via intrinsic image decomposition with facial priors. *IEEE Transactions on Pattern Analysis and Machine Intelligence 41*, 6 (2019), 1455–1469. doi:10.1109/TPAMI.2018.2832059. 2, 3

[MPG*16] MÜLLER T., PAPAS M., GROSS M., JAROSZ W., NOVÁK J.: Efficient rendering of heterogeneous polydisperse granular media. *ACM Transactions on Graphics 35*, 6 (2016), 168:1–168:14. doi:10.1145/2980179.2982429. 2

[MPH*15] MENG J., PAPAS M., HABEL R., DACHSBACHER C., MARSCHNER S., GROSS M., JAROSZ W.: Multi-scale modeling and rendering of granular materials. *ACM Transactions on Graphics 34*, 4 (July 2015), 49:1–49:13. doi:10.1145/2766949. 2

[MPR05] MAILE F. J., PFAFF G., REYNDERS P.: Effect pigments—past, present and future. *Progress in Organic Coatings 54*, 3 (11 2005), 150–163. doi:10.1016/j.porgcoat.2005.07.003. 3

[MTH09] MORIUCHI Y., TOMINAGA S., HORIUCHI T.: *Precise Analysis of Spectral Reflectance Properties of Cosmetic Foundation*, vol. 5575 LNCS. 2009, pp. 138–148. doi:10.1007/978-3-642-02230-2_15. 2, 6

[MWAM05] MARSCHNER S. R., WESTIN S. H., ARBREE A., MOON J. T.: Measuring and modeling the appearance of finished wood. *ACM Transactions on Graphics 24*, 3 (2005), 727–734. doi:10.1145/1073204.1073254. 2

[NL17] NGUYEN T. V., LIU L.: Smart mirror: intelligent makeup recommendation and synthesis. In *Multimedia (MM '17)* (2017), ACM, pp. 1253–1254. doi:10.1145/3123266.3127926. 2

[NNN*22] NIKLASSON G. A., NIKLASSON S. L., NOTFORS C., WANG J., STRØMME M., ÅRHAMMAR C.: Optics of sunscreen lotions: Preliminary results on scattering and absorption coefficients. arXiv:2204.13507 [physics.med-ph], 2022. doi:10.48550/arXiv.2204.13507. 5

[PdMJ14] PAPAS M., DE MESA K., JENSEN H. W.: A physically-based BSDF for modeling the appearance of paper. *Computer Graphics Forum 33*, 4 (2014), 133–142. doi:10.1111/cgf.12420. 2

[PFG00] PELLACINI F., FERWERDA J. A., GREENBERG D. P.: Toward a psychophysically-based light reflection model for image synthesis. In *Proceedings of SIGGRAPH 2000* (2000), pp. 55–64. doi:10.1145/344779.344812. 7, 8

[PJH23] PHARR M., JAKOB W., HUMPHREYS G.: *Physically Based Rendering: From Theory to Implementation*. MIT Press, 2023. doi:10.5555/3044800. 5, 7

[SLH*19] SHIRLEY P., LAINE S., HART D., PHARR M., CLARBERG P., HAINES E., RAAB M., CLINE D.: *Sampling Transformations Zoo*. Apress, Berkeley, CA, 2019, pp. 223–246. doi:10.1007/978-1-4842-4427-2_16. 5

[SLL*20] SUN Z., LIU F., LIU W., XIONG S., LIU W.: Local facial makeup transfer via disentangled representation. In *Asian Conference on Computer Vision (ACCV)* (2020), Springer, pp. 8538–8551. doi:10.1007/978-3-030-69538-5_28. 2

[SRH*11] SCHERBAUM K., RITSCHEL T., HULLIN M., THORMÄHLEN T., BLANZ V., SEIDEL H.-P.: Computer-suggested facial makeup. *Computer Graphics Forum 30*, 2 (2011), 485–492. doi:10.1111/j.1467-8659.2011.01874.x. 2

[Sta01] STAM J.: An illumination model for a skin layer bounded by rough surfaces. In *Rendering Techniques 2001 (EGWR 2001)*. Springer, 2001, pp. 39–52. doi:10.1007/978-3-7091-6242-2_4. 2

[TLAV23] TRAN L., LALANNE P., ASKENAZI B., VYNCK K.: Physically based modeling of the colored appearance of complex media for cosmetics. In *Proceedings of the 33rd IFSCC Congress* (Barcelona, Spain, September 2023). 10

[TM09] TOMINAGA S., MORIUCHI Y.: Principal component analysis-based reflectance analysis/synthesis of cosmetic foundation. *Journal of Imaging Science and Technology 53*, 6 (2009), 60403–1–60403–8. doi:10.2352/J.ImagingSci.Technol.2009.53.6.060403. 2

[TS67] TORRANCE K. E., SPARROW E. M.: Theory for off-specular reflection from roughened surfaces. *Journal of the Optical Society of America 57*, 9 (1967), 1105–1114. doi:10.1364/JOSA.57.001105. 2

[War92] WARD G. J.: Measuring and modeling anisotropic reflection. *Computer Graphics (SIGGRAPH '92) 26*, 2 (1992), 265–272. doi:10.1145/133994.134078. 6

[Wat09] WATTS I.: Red ochre, body painting, and language: interpreting the blombos ochre. *The cradle of language 2* (2009), 93–129. doi:10.1093/oso/9780199545858.003.0004. 1

[WB20] WEIER P., BELCOUR L.: Rendering layered materials with anisotropic interfaces. *Journal of Computer Graphics Techniques 9*, 2 (June 2020), 37–57. URL: http://jcgt.org/published/0009/02/03/. 2

[WCA*22] WAN Z., CHEN H., AN J., JIANG W., YAO C., LUO J.: Facial attribute transformers for precise and robust makeup transfer. In *Winter Conference on Applications of Computer Vision (WACV)* (2022), IEEE, pp. 1717–1726. doi:10.1109/WACV51458.2022.00317. 2

[WJHY22] WANG B., JIN W., HAŠAN M., YAN L.-Q.: Spongecake: A layered microflake surface appearance model. *ACM Trans. Graph. 42*, 1 (sep 2022). doi:10.1145/3546940. 2, 10

[WSZT21] WARGALA E., SŁAWSKA M., ZALEWSKA A., TOPOROWSKA M.: Health effects of dyes, minerals, and vitamins used in cosmetics. *Women 1*, 4 (2021). doi:10.3390/women1040020. 3

[WW07] WEIDLICH A., WILKIE A.: Arbitrarily layered micro-facet surfaces. In *GRAPHITE* (2007), ACM, pp. 171–178. doi:10.1145/1321261.1321292. 2

[WXN*19] WANG J., XU C., NILSSON A. M., FERNANDES D. L. A., NIKLASSON G. A.: A novel phase function describing light scattering of layers containing colloidal nanospheres. *Nanoscale 11*, 15 (2019), 7404–7413. doi:10.1039/C9NR01707K. 5

[XDZ13] XU L., DU Y., ZHANG Y.: An automatic framework for example-based virtual makeup. In *International Conference on Image Processing (ICIP)* (2013), IEEE, pp. 3206–3210. doi:10.1109/ICIP.2013.6738660. 2

[XWHM20] XIA M., WALTER B., HERY C., MARSCHNER S.: Gaussian product sampling for rendering layered materials. *Computer Graphics Forum 39*, 1 (2020), 420–435. doi:10.1111/cgf.13883. 2

[YGZ*23] YAN Q., GUO C., ZHAO J., DAI Y., LOY C. C., LI C.: BeautyREC: robust, efficient, and component-specific makeup transfer. In *Computer Vision and Pattern Recognition (CVPR)* (2023), IEEE, pp. 1102–1110. doi:10.1109/CVPRW59228.2023.00117. 2

[YHXG22] YANG C., HE W., XU Y., GAO Y.: EleGANt: Exquisite and locally editable GAN for makeup transfer. In *European Conference on Computer Vision (ECCV)* (2022), Springer, pp. 737–754. doi:10.1007/978-3-031-19787-1_42. 2

[YLHS20] YAN Y., LEE J., HONG J., SUK H.: Measuring and describing the discoloration of liquid foundation. *Color Research and Application 46*, 2 (2020), 362–375. doi:10.1002/col.22584. 6

[YO21] YOSHIDA K., OKIYAMA N.: Estimation of reflectance, transmittance, and absorbance of cosmetic foundation layer on skin using translucency of skin. *Opt. Express 29*, 24 (Nov 2021), 40038–40050. doi:10.1364/OE.442219. 7

[YTK23] YANG X., TAKETOMI T., KANAMORI Y.: Makeup extraction of 3D representation via illumination-aware image decomposition. *Computer Graphics Forum 42*, 2 (2023), 293–307. doi:10.1111/cgf.14762. 2

[ZJ18] ZELTNER T., JAKOB W.: The layer laboratory: a calculus for additive and subtractive composition of anisotropic surface reflectance. *ACM Transactions on Graphics 37*, 4 (2018), 74:1–74:14. doi:10.1145/3197517.3201321. 2

[ZJA*23] ZHU J., JARABO A., ALIAGA C., YAN L.-Q., CHIANG M. J.-Y.: A realistic surface-based cloth rendering model. In *ACM SIGGRAPH 2023 Conference Proceedings* (2023), pp. 5:1–5:9. doi:10.1145/3588432.3591554. 2

[ZJMB11] ZHAO S., JAKOB W., MARSCHNER S., BALA K.: Building volumetric appearance models of fabric using micro CT imaging. *ACM Transactions on Graphics 30*, 4 (2011), 44:1–44:10. doi:10.1145/2010324.1964939. 2

Parameter	Dewy 1	Dewy 2	Matte 1	Matte 2
α_p	0.13	0.002	0.15	0.49
θp	1.47°	5.5°	2.01°	52.2°
Λ_p	(0.75,0.85,0.99)	(0.8,0.8,0.8)	(0.91, 0.89,0.85)	(0.93,0.83,0.71)
c_d	0.90	0.99	0.89	0.29
Λ_d	(0.99,0.98,0.95)	(0.97,0.93,0.87)	(0.95,0.94,0.91)	(0.9,0.9,0.84)
g_1	0.55	0.77	0.37	0.24
g_2	0.09	-0.23	-0.25	-0.22
w_g	1.0	0.79	0.62	0.51
t	16	16	16	16

Table 2: *Optimized parameters fit from our measured reflectance data using our cosmetic appearance model for several cosmetic products.*

Figure	Resolution	SPP	Time	Thickness
7 (First row - Matte 1)	1223×1269	128	11.4 min	0.5
7 (First row - Matte 2)	1223×1269	128	11.0 min	0.5
7 (First row - Reference)	1223×1269	128	9.25 min	0.5
7 (First row - Dewy 1)	1223×1269	128	9.95 min	0.5
7 (First row - Dewy 2)	1223×1269	128	10.95 min	0.5
7 (Second row - Matte 1)	1332×1187	512	25.3 min	0.35
7 (Second row - Matte 2)	1332×1187	512	24.8 min	0.35
7 (Second row - Reference)	1332×1187	512	24.8 min	0.35
7 (Second row - Dewy 1)	1332×1187	512	24.2 min	0.35
7 (Second row - Dewy 2)	1332×1187	512	25.3 min	0.35
11 (First row - no foundation)	1332×1187	512	25.3 min	0.0
11 (First row - one layer)	1332×1187	512	25.3 min	0.25
11 (First row - two layers)	1332×1187	512	25.3 min	1.25

Table 3: *Rendering times for the the figures in the paper.*

Appendix A: Optimized Parameters and Rendering Time

In the following, we report the optimized parameters (see Table 2) for the four foundation samples measured and renderings time for some of the figures in Table 3. Notice how our cosmetic layer only introduces a small overhead in terms of rendering time despite our work being more focused on rendering accuracy than computational performance and we do not perform any sophisticated performance optimization strategies.